Int J Adv Manuf Technol (2014) 70:1847–1857
DOI 10.1007/s00170-013-5416-9

ORIGINAL ARTICLE

Characterisation and modelling of behaviour of a shape memory alloys

Mohamed Lakhdar Sahli · Brahim Necib

Received: 2 July 2013 / Accepted: 7 October 2013 / Published online: 1 November 2013

Abstract Shape memory alloys (SMAs) provide an attractive solid-state actuation alternative to engineers in various fields due to their ability to exhibit recoverable deformations while under substantial loads. This feature is of particular importance when utilising the smart composite materials reinforced by SMA. Many constitutive models describing this repeatable phenomenon have been proposed, where some models also capture the effects of rate-independent irrecoverable deformations in SMAs. This paper presents experimental investigations and numerical simulations on shape memory alloys. First, by consisting in determining the transformations of equiatomic Ti–Ni shape memory alloys by differential scanning calorimeter. Then, in order to validate a 3D numerical model of the pseudoelastic behaviour of SMA allowing a finite strain analysis, a set of experimental tests at various initial temperatures is proposed. Finally, the numerical simulations of uniaxial tests performed on shape memory alloys are presented and compared with experimental data, permitting the validation of the proposed modelling. Reasonably good correlation is obtained between the experimental and model predictions.

Keywords Shape memory alloys · Finite element analysis · Differential scanning calorimetry · Modelling · Large deformation · Constitutive modelling

M. L. Sahli (✉)
Applied Mechanics Department, Femto-ST Institute,
CNRS UMR 6174, ENSMM, 25030 Besançon, France
e-mail: mohamed.sahli@ens2m.fr

B. Necib
Laboratory of Mechanics, Faculty of Engineering Sciences,
Mentouri-Constantine University, Road of Ain-el-Bey, 25000,
Constantine, Algeria

1 Introduction

The shape memory alloys (SMAs) are known to exhibit unique thermomechanical characteristics, such as the shape memory effect, superelasticity, pseudo-elasticity, or large recoverable stroke (strain), high-damping capacity and adaptive properties which arise due to a reversible martensitic transformation, occurring at the solid state between two phases, the so-called austenite and martensite [1–5]. The important characteristics of these alloys are their ability to exist in two distinct shapes or configurations above or below a certain critical transformation temperature. It undergoes diffusionless martensitic transformation, which is also thermo elastic in nature; below the critical temperature, a martensitic structure forms and grows as the temperature is lowered, whereas on heating, the martensite shrinks and ultimately vanishes [6, 7]. The SMAs are now used in applications in a wide variety of devices ranging from simple parts like cell phone antennas or eyeglass frames to complicated devices in mechanical [8–11], biomechanical [12], aerospace [13], and civil engineering [14].

Currently, the shape memory alloys are one of the major elements of intelligent/smart composites because of their unusual properties, such as adaptive properties which are due to the (reversible) phase transitions in the materials (see Fig. 1). SMAs may sense thermal or stress stimulus and exhibit actuation or some pre-determined response, making it possible to tune some technical parameters such as shape, position, strain, stiffness, natural frequency, damping, and other static and dynamical characteristics of material systems in response to the environmental changes. The martensitic transformation may be induced by a change, either in the applied stress, the temperature, or both [15–27]. The transformation deformation mechanism is schematically illustrated in Fig. 2. The initial austenite phase can be transformed into martensitic phase under external force. Due to different crystal structures between the

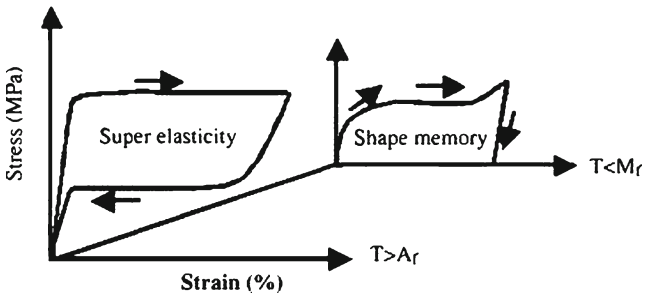

Fig. 1 Stress/strain behaviour of SMA: **a** shape memory effect and **b** superelastic effect

austenite and the martensite, deformation occurs during the phase transformation process, which leads to significant macroscopic deformation. Once the transformed material is unloaded, the unstable martensitic phase will transform backward to the stable austenite recovering the transformation strain.

Recent numerous research efforts have focused on Ti–Ni SMAs because of their good memory properties and low-production cost. The works of others have also examined high-stress rate-independent yielding plasticity in SMAs that occurs when local-resolved stresses exceed those required to initiate slip [28–33]. The work of Hartl and Lagoudas [33], for example, considers the simultaneous evolution of transformation and plastic strains.

Various mathematical analysis and numerical simulation of the behaviour of shape memory alloys have received considerable attention during the last 10 years. A large effort has been made by many researchers to introduce more precise analytical and numerical methods for analysing pseudoelastic and SME response of SMA structures. Some of these studies focus on introducing constitutive equations to model SMA response to mechanical and thermal loads more accurately [34–36] while others focus on numerical, semi-analytical [37], and exact solutions [38].

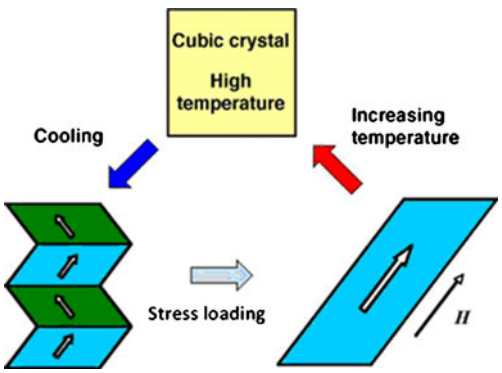

Fig. 2 Illustrating superelastic deformation mechanism

In order to explain and describe the complex phenomena of shape memory alloys, a series of constitutive models have been developed [39–42]. In general, the models can be classified into two categories. One is built upon macroscopic observation [39, 43, 44]. This class of models is simpler in formulation and easier to implement into finite element analysis [40–42]. The other class is based on the micromechanics of a single crystal [45–47]. This class of model is based on a kinematical description of the physical strain mechanism.

Auricchio and Taylor [48] developed a constitutive model which reproduces the superelastic behaviour of shape memory alloys at finite strains by using a modelling and numerical simulation. They have implemented a thermomechanical model able to simulate also the shape memory effect and the reorientation process for the single-variant martensites. The proposed approach conducted to simulate the response of some simple SMA-typical structures as well as an application with possibly a very high impact in different medical fields (SMA stent,…etc.). Past investigations of finite element modelling of SMA structures has been previously discussed and addressed by Brinson and Lammering [51]. Also, the constitutive theory based on Tanaka's model [53, 54], modified by Brinson [50], has been employed to describe the SMA behaviour. Auricchio and Taylor [48, 49] have also proposed a three-dimensional finite element model. Kouzak et al. [52] also treats SMA beams using a constitutive equation proposed by Brinson [50]. The phenomenological models have the advantage that their material parameters can be usually identified by classical experimental tests and the structure of their material equations is mostly well suited to be implemented into computer programmes for structural analyses as finite element programmes [34, 39, 44, 55–57]. The aim of this paper is to present and discuss some of the results concerning the experimental and numerical validation of superelastic response of polycrystalline Ti–Ni material under tension loading.

2 SMA constitutive model

To observe the mechanical characterization of the tensile specimens, a 3D uniaxial tension finite element model is built. Larger-sized meshes are adopted at the clamping zone of the specimens, while smaller-sized meshes are adopted at the tensile zone, and the meshes at the middle zone of the specimens are refined. In this study, tensile specimen made from a Ti–Ni alloy is considered to undergo uniaxial isothermal tension and there are 1,088 elements with 2,394 nodes total in the model. However, the plane stress conditions for thin tensile specimens are assumed to exist (see Fig. 3).

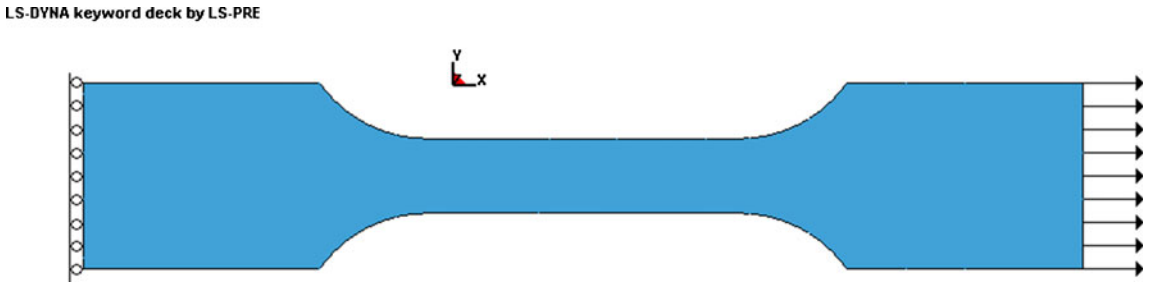

Fig. 3 Schematic of isothermal uniaxial tension loading

The elements used for the mesh are eight-node linear brick hybrid element, contains 24 degrees of freedom collectively representing the linear displacements at each of the element nodes. Initially, the material is nickel–titanium shape memory alloy in the austenitic state.

In order to investigate the superelastic behaviour of Ti–Ni SMA, numerical simulations with the commercial-explicit FE code LS-Dyna® were used. The material model used for the SMA material modelling of the tensile sample is MAT_SHAPE_MEMORY. It describes the superelastic response present in shape memory alloy, which is the peculiar material ability to undergo large deformation with a full recovery in loading and unloading cycle (see Fig. 4). The one-dimensional stress–strain relation is generally written as:

$$\sigma - \sigma_0 = E(\varepsilon - \varepsilon_0) + \Omega(\xi_s - \xi_{s0}) + \theta(T - T_0) \tag{1}$$

where E is Young's modulus, Ω is transformation coefficient, ξ_s is stress-induced martensite volume fraction, θ is thermal elastic coefficient and T is temperature. The subscript '0' indicates the initial values. Ω is expressed as:

$$\Omega = -\varepsilon_L E \tag{2}$$

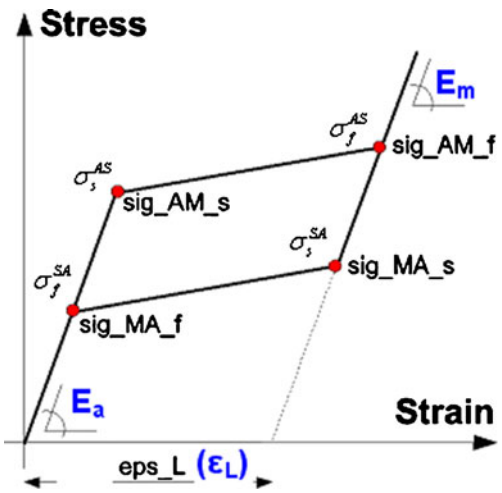

Fig. 4 Stress–strain relationship exhibited by the superelastic shape memory alloy constitutive model. Sketch of the material response under tensile loads

where ε_L is the maximum residual strain. Young's modulus E is a function of the martensite volume fraction ξ, which is given by:

$$E = E_a - \xi(E_m - E_a) \tag{3}$$

where E_m and E_a are Young's modulus of austenite and martensitic phases, respectively. The total martensite volume fraction ξ is expressed as:

$$\xi = \xi_s - \xi_T \tag{4}$$

where ξ_T is the temperature-induced martensite volume fraction. ξ, ξ_s and ξ_T are functions of the temperature T and the stress σ.

To the boundary condition, one end is fixed and the other end is applied with an initial velocity of 0.1 mm/min. Figure 4 shows the boundary conditions. The material parameters of the models are listed in Table 1.

3 Material and experimental methods

3.1 Material

This experimental study has been realised on a Ti–Ni (Ti 50.51 Ni 49.49 in atomic percent) polycrystalline SMA. For the calorimetric measurements, a dozen specimens were cut from the Ti–Ni plate and submitted to thermomechanical

Table 1 Materials parameters for modelling

Ti–Ni	Austenitic [100 %]	Martensitic [100 %]
Density	4.5	4.5
Young's modulus [MPa]	58,334	25,000
Poisson's ratio	0.3	0.3
σ_f^{AS} [MPa]	350	175
σ_s^{AS} [MPa]	475	100
σ_f^{SA} [MPa]	250	60
σ_s^{SA} [MPa]	175	25
ε_L [%]	0.06	0.06

treatment. The dimension of plate Ti–Ni SMA was 100 × 100 × 3.5 mm. Table 1 shows the key physical properties of equiatomic Ti–Ni SMA. The specimens were heat treated at 870 °C for 2 h (quenching), followed by annealing at different temperatures: 265, 350, 425 and 520 °C vs. time in a furnace, and then cooled to room temperature in air (Fig. 5).

3.2 Experimental procedures

The properties of Ti–Ni SMAs, including transformation temperatures, mechanical properties and some other interesting aspects were studied by differential scanning calorimetry (DSC) and tensile testing. DSC was conducted using a system Setaram (DSC92) thermal analyzer equipped with a quantitative scanning system 910 DSC cell to control the heating and cooling rates on samples encapsulated in an aluminium pan. Test temperatures ranged from −60 to 150 °C with a heating/cooling rate of 10 °C/min. The specimens were weighed, and then placed into standard Al-specimen pans. Subsequently, the Ti–Ni specimens, about 20 mg in weight, were treated at different heating/cooling rates in the DSC apparatus. Figure 6 shows a schematic representation of the evolution of typical DSC measurements of the reverse transformation behaviour of Ti–Ni.

The tensile tests were performed at different temperatures ($T < M_f$ or $T > A_f$) with an Instron 6025 testing electrical machine operating in axial strain control. This machine was equipped with a 100-kN force cell. The loading rate is 0.1 mm/min, which is assumed to be sufficiently slow for the evolution to remain quasi-static and isothermal. The tests are conducted at two different ambient temperatures, namely 40 and 90 °C. Their elongation was measured by an extensometer.

Each specimen was loaded to the level above the transformation limit and then unloaded with the same rate of deformation. The stress/strain curves obtained at 40 and 90 °C

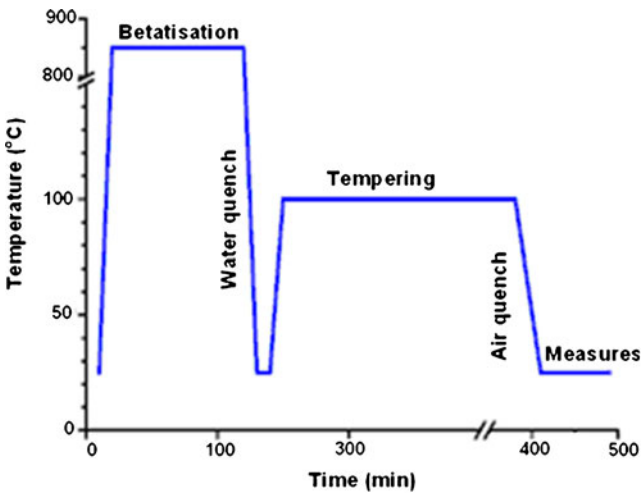

Fig. 5 Schematic illustration of a heat treatment

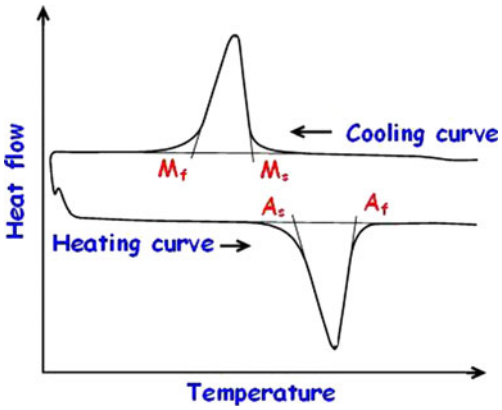

Fig. 6 A typical DSC Curve for a Ti–Ni shape memory alloy

were used for determining the conventional yield stress of the martensite and the phase yield strength of the austenite, respectively. Figure 7a show the test piece geometry used in the present investigation. The investigations were performed on the same plate specimen. The Ti–Ni samples used in this study were heat treated to eliminate work hardening from the manufacturing process. Figure 7b shows photography of a tensile testing machine.

4 Experimental resultants

4.1 Transformation behaviour of Ti–Ni alloys

To investigate the behaviours of Ti–Ni alloys, it is helpful to first understand some important metallurgical properties of these alloys. From the DSC curves, the transformation start and finish temperatures were determined. Here, M_s and M_f are the start and finish temperature of forward martensitic transformation, respectively. A_s and A_f are those of reversed martensitic transformation, respectively (see Fig. 6).

The DSC curves presented in Fig. 8 correspond to the forward and reverse martensitic transformation of the Ti–Ni-

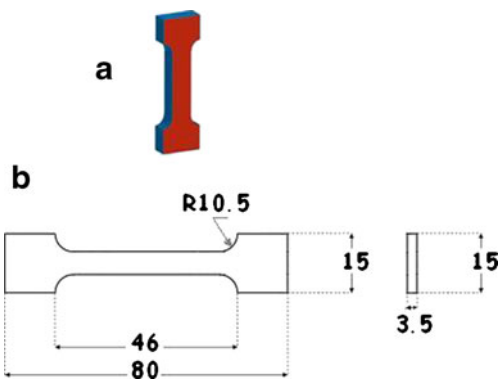

Fig. 7 The dumbbell type test piece used for tensile testing: **a** perspective view, **b** dimensions

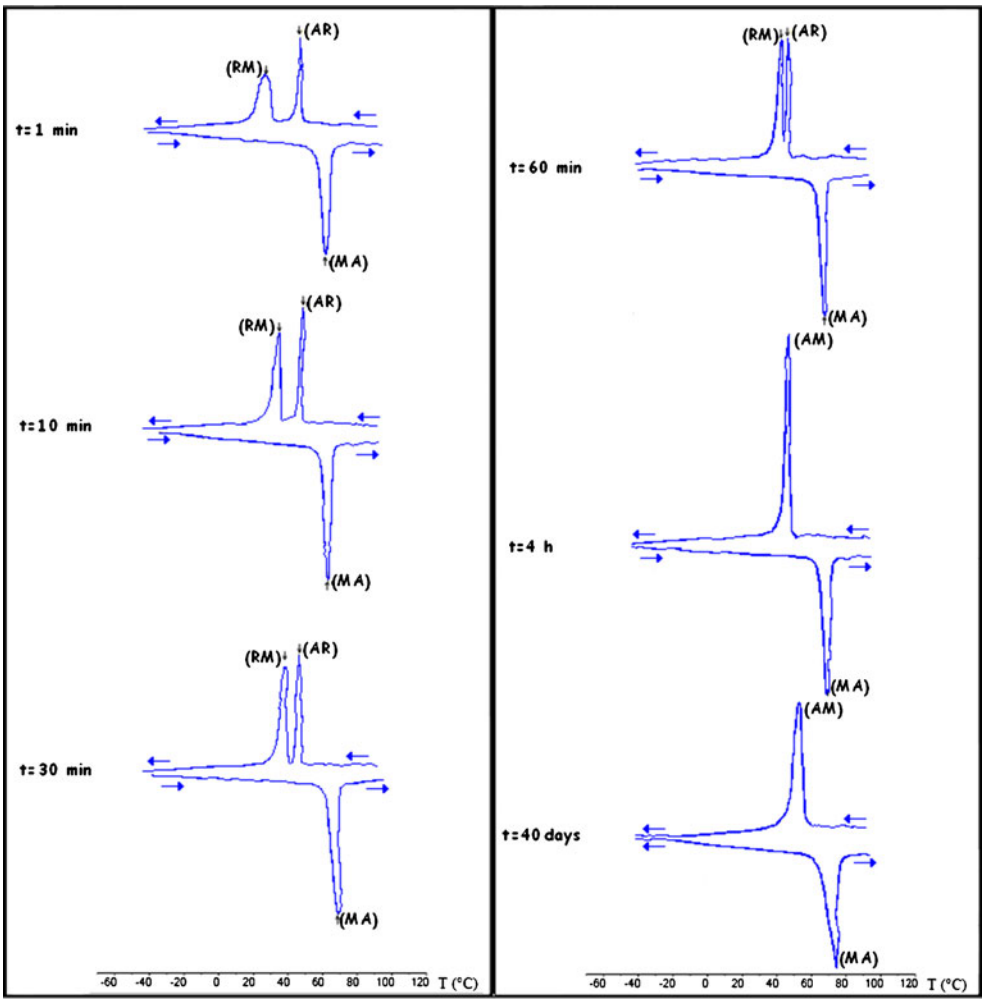

Fig. 8 DSC measurement of Ti–Ni sample annealed at 520 °C

studied alloys after the treatment. It shows the DSC curves of specimen vs. time during heating/cooling. Apparently, while heating the specimen produces one endothermic peak; cooling the specimen creates two exothermic peaks which indicate the A → R → M transformation. It can be seen clearly that the effect of duration of heat treatment on the transformation temperatures are remarkably different. A highly deformed sample after annealing at 525 °C during 1 min, shows the martensitic transformation: At cooling stage, it appears as two well-separated peaks corresponding to the austenite transformation—R phase: peak (AR) and R phase—martensite: peak (RM), respectively. One can also observe a broad peak (RM), while the peak (AR) is narrower and better defined. At heating stage, a single peak is present, it is associated with the reverse transformation martensite—austenite peak (MA).

As an example, the peak (MA) is refined and temperature changes have little effect when increasing time. Therefore, the peak (RM) apparently is most sensitive, while the peak (AR) is hardly changing. The peak (RM) is more refined with an increasing temperature.

The effect of annealing heat-treatment temperature on the different peaks of transformation temperature has been studied. As an example, a peak evolution of MA is plotted in Fig. 9. It was noted that the peak temperature (MA) has changed little. Concerning both peaks' temperature (AR) and (RM), it was also found that the peak (AR) doesn't change substantially. However, the effect is very important on the peak temperature (RM). The results in Fig. 10 correspond to the hysteresis of martensitic transformation, defined as the difference in temperature between the peaks (MA) and (RA) or (RM). During annealing, it systematically decreases with increasing time and returns to its initial value (≈30 °C) of the normalised.

Several heat treatments were investigated in order to modify the transformation temperatures of alloys. The objectives were to dislocate the critical temperatures for near-room temperature and to avoid the R phase formation, which is very common in Ti–Ni alloys. Finally, a heat treatment (a quenching at 870 °C for 2 h, followed by annealing at 520 °C during 4 h and then cooled to room temperature in air), was chosen on which, R phase is absent.

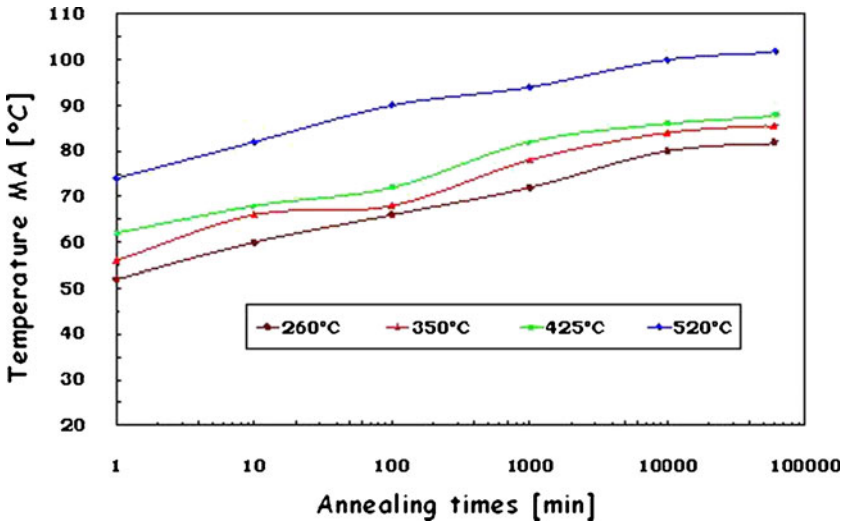

Fig. 9 Evolution of the MA peak width

The main advantage of suppressing the R phase formation is to attain uniformity in the stress fields, proportioning a better efficiency of the shape memory effect.

4.2 Physical and mechanical characterization

The mechanical characteristics registered during the tensile test make it possible to derive the stress/strain relations. The tests were performed using five repeats per sample set. Figure 11 shows a nonlinear response with a maximum strain of 7.15 % reached and the strain was fully recovered. At temperatures T=40 °C ($T < M_f$), the deformation related to martensitic transformation; the rearrangement of martensite amounts to about 6.9 % when the stress increases to 175± 5 MPa. Tensile tests were also carried out for the same specimen at temperature T=90 °C ($T > A_f$). It can be seen from Fig. 11 that in the case of 100 % initially austenitic ($T > A_f$), the stress increases quickly and the slope of the stress/strain curve is rather steep at the beginning, but when the stress gets to about 350±5 MPa, the alloy starts to yield, causing the stress to rise slowly and the strain to increase substantially at the same time. When unloaded at 475±5 MPa, the stress drops rapidly during the first stage and then the rate of decrease decelerates when the stress drops to 175±5 MPa. After full unloading, the strain returns to zero.

4.3 Numerical results and discussions

The simulation has been performed using the hyperelastic behaviour available in the calculation codes LS-DYNA®. This model takes into consideration the difference of the Young's modulus between the austenite and martensite phases. This difference is also obvious according to experimental data. The difference of the Young's modulus between austenitic and martensitic phases has been considered.

Concerning the stress isovalues, it may be shown that high-stress σ_{xx} values are mainly located at the useful part of the tensile test specimen (Figs. 12 and 13). Figures 12 and 13

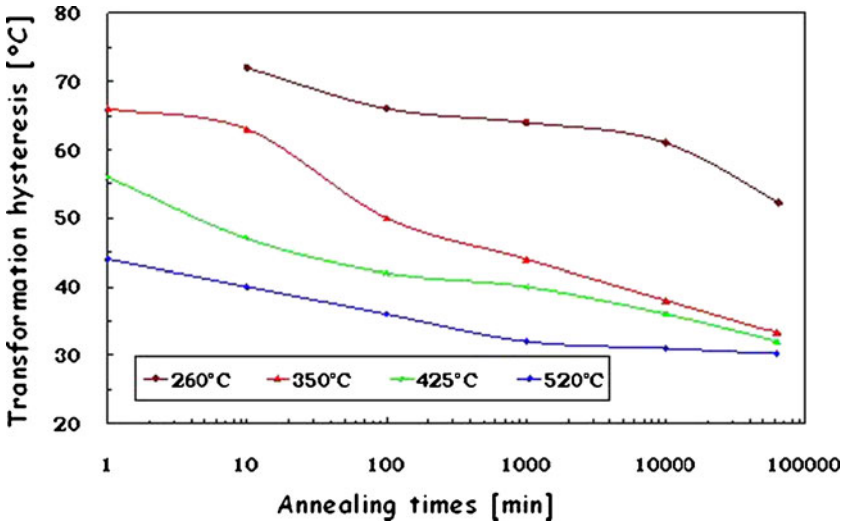

Fig. 10 Evolution of temperature hysteresis of martensitic transformation

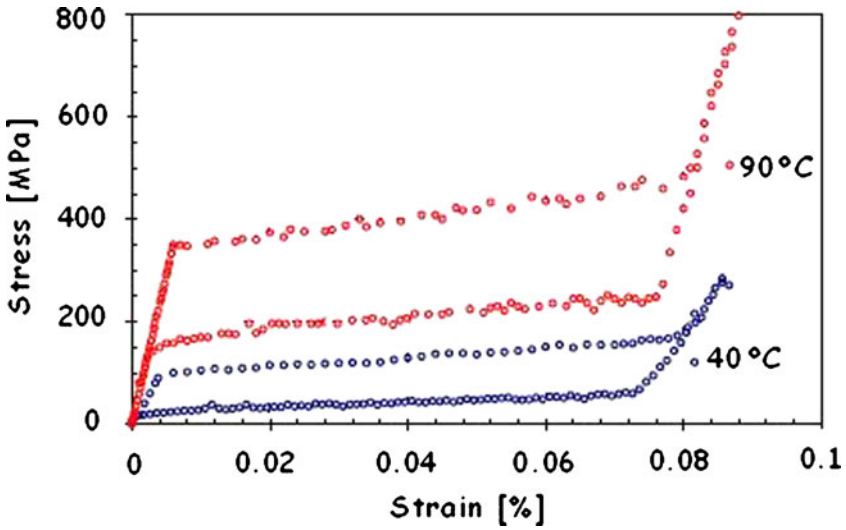

Fig. 11 Axial stress versus axial strain curve of Ti–Ni SMA under uniaxial tension and strained at temperatures 40 and 90 °C with travel speed 0.1 mm/min

shows a contour plot of Von Mises strain isovalues in SMA samples at different temperatures along direction x.

Figure 12 related that this simulation reproduces well the different stages of loading the specimen. The Von Mises stress fields are given for two different times. The simulation results are consistent with respect to the geometric changes of the specimens during deformation. For the superelastic behaviour of SMA sample, the simulation result is shown in Fig. 13 which relates isovalues of Von Mises stresses. In this configuration, it was found that the results are very different from the previous case (Fig. 12). Indeed, the calculated stresses in the case of a superelastic behaviour of austenitic SMA are significantly higher than in the case of the shape memory effect and this is due to the difference value of Young's modulus in the two phases.

Figure 14 shows the temperature distributions with a strain rate of 0.1 mm/min. There is an increasing temperature during the tensile test and a maximum temperature of 90 °C localised in the central zone of the useful part of the specimen. Moreover, the results clearly indicate the effect of taking into account the coupled thermal stress. Note that the thermo-mechanical coupling increases the ductility of the material.

4.4 Experimental validation

The simulation result is compared with the tensile test result for SMA sample in Figs. 15 and 16 in order to verify the finite element model. These figures show good agreement between simulated and experimental behaviours. As an example, the

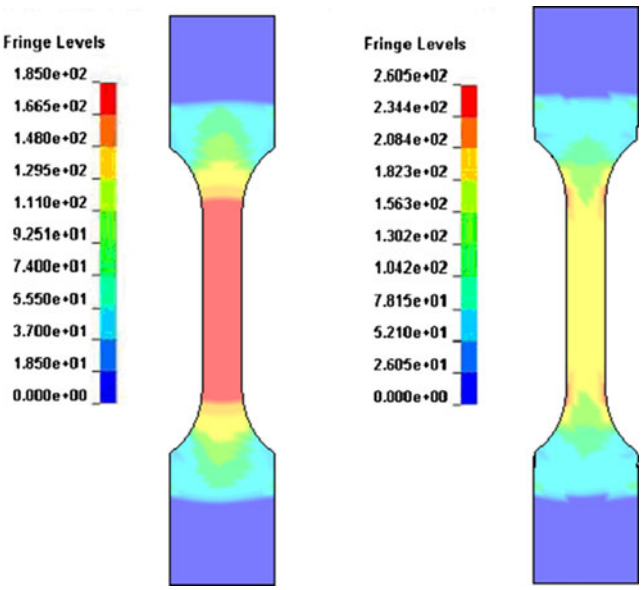

Fig. 12 Contour plot of Von Mises strain isovalues in martensitic sample along tension direction *x*

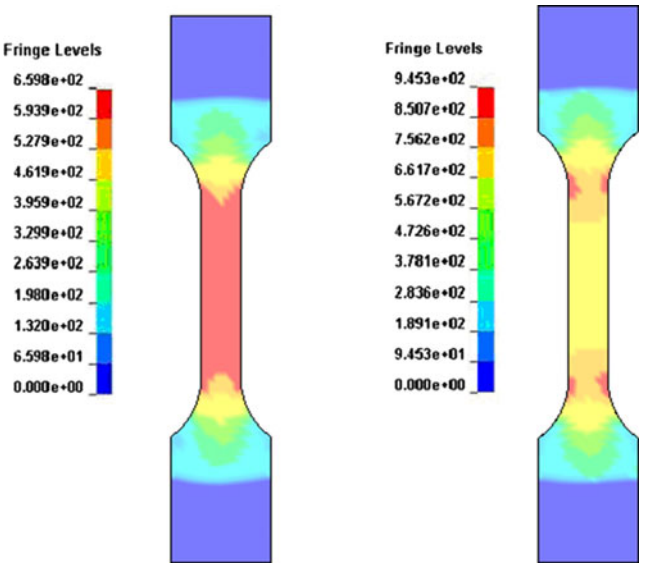

Fig. 13 Contour plot of Von Mises strain isovalues in austenitic sample along tension direction *x*

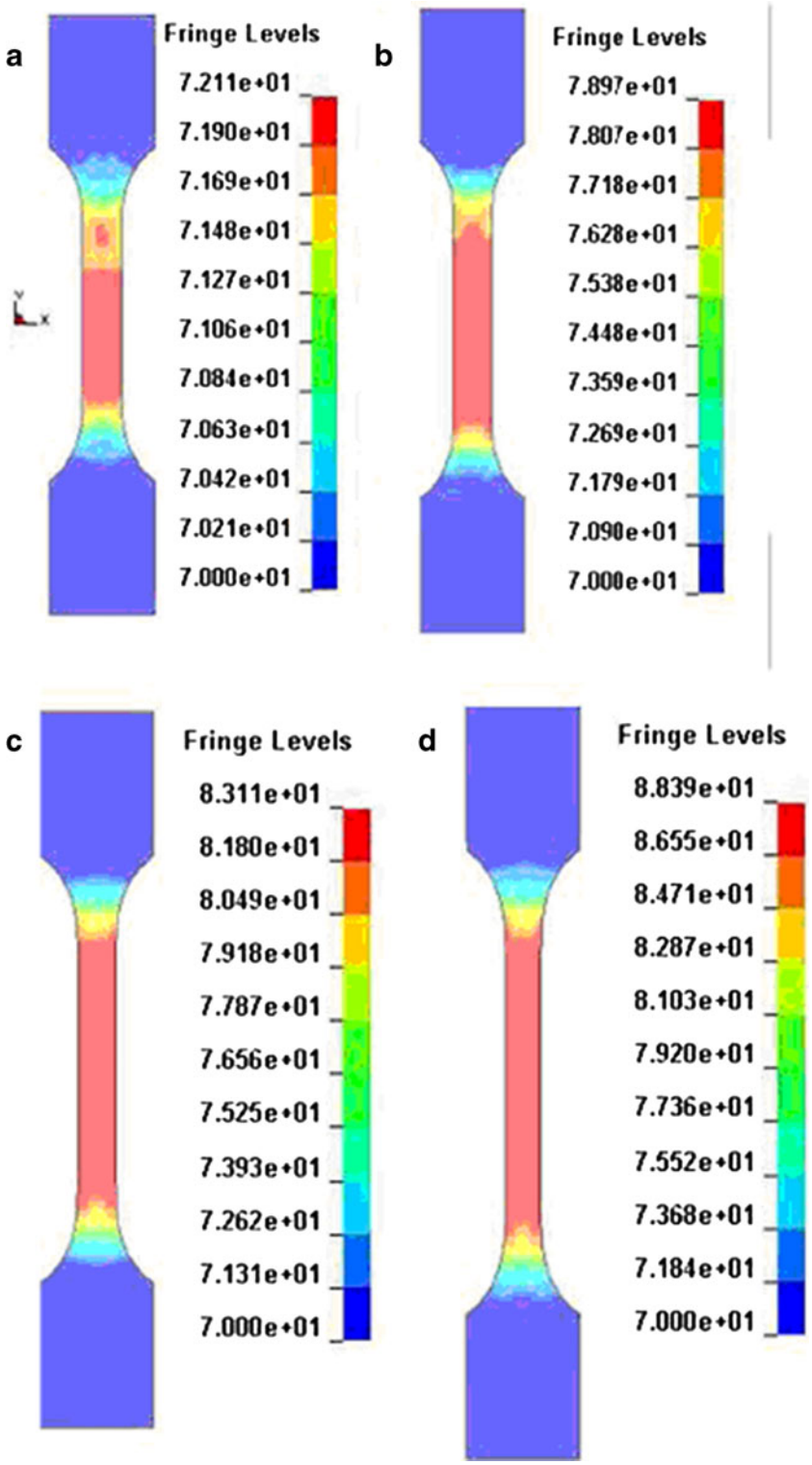

Fig. 14 Contour plot of the temperature evolution in the austenitic tensile sample

simulated martensitic transformation start and finish stress of sample, 352±2 and 478±2 MPa, are slightly higher than the experiment result. While the case for reverse transformation start and finish stress of sample, 244±2 and 182±2 MPa. The elongation (ε_L) obtained by simulation in both states (sample with various initial 100 % of austenite grain size or 100 % of martensite) are equal to 0.1 and 0.4 %, respectively, are higher than the experiment.

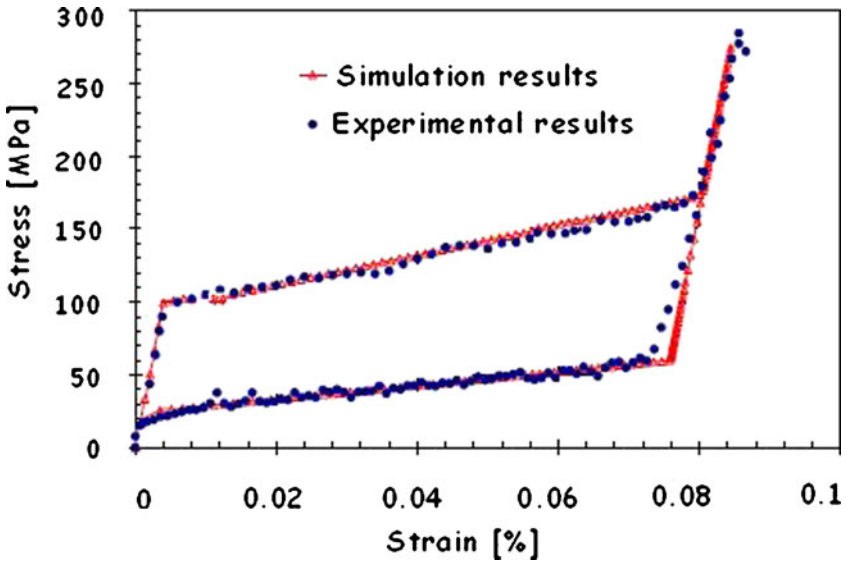

Fig. 15 Comparison of experimental result and simulation result of SMA simple at 40 °C

5 Conclusions

In this paper, a general inelastic framework for the development of a one-dimensional constitutive model for materials undergoing phase transformations and in particular, shape memory alloys has been proposed. The more noteworthy results of the study are:

1. The effect of annealing heat-treatment temperature on the different peaks of transformation temperature has been investigated using DSC. We have seen clearly that the duration of heat treatment is sensibly affected by the transformation temperatures. However, the heat treatment of a quenching at 870 °C for 2 h, followed by annealing at 520 °C during 4 h and then cooled to room temperature in air, was chosen to dislocate the critical temperatures for near-room temperature. It also leads to avoid the R phase formation in Ti–Ni alloys,
2. A number of tensile tests have been performed in order to understand the thermo-mechanical response, especially the hyperelastic behaviour of Ti–Ni SMAs. The calculated stresses in the case of a superelastic behaviour of austenitic SMA are significantly higher than in the case of the shape memory effect, the order of 3.5 % and the strain were fully recovered,
3. Several numerical simulations were also presented and experimental validation proved to be successful in the case of uniaxial thermomechanical loading. The stress/strain curves obtained from several uniaxial superelastic experiments conducted on a polycrystalline sample Ti–Ni were well predicted by the constitutive model and the finite element simulations. The constitutive model is also

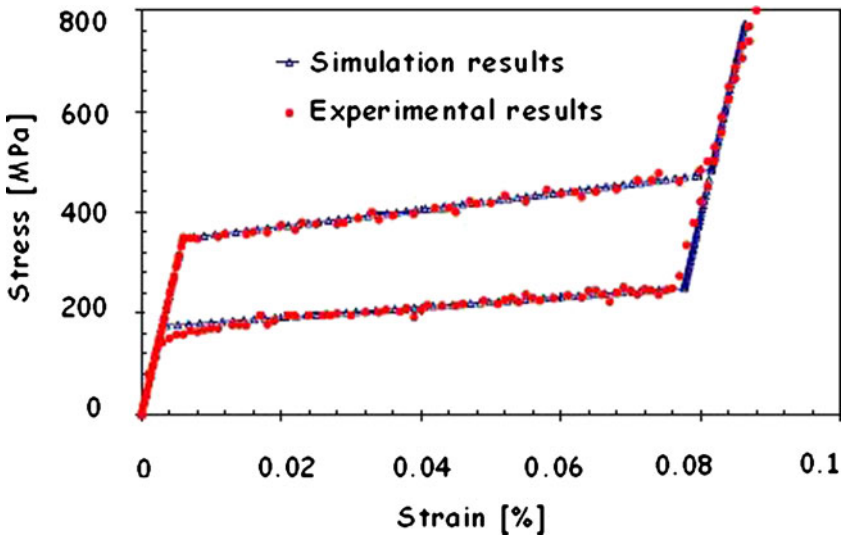

Fig. 16 Comparison of experimental result and simulation result of SMA simple at 90 °C

able to qualitatively reproduce the experimental strain/temperature cycling and one-way shape memory effect responses exhibited by shape memory alloys. The overall agreement was quite good.

According to this work, a modelling and development of smart composites may be possible by using this model for SMA wires.

References

1. Nemat-Nassera S, Sua Y, Guob W-G, Isaacsa J (2005) Experimental characterization and micromechanical modeling of superelastic response of a porous NiTi shape-memory alloy. J Mech Phys Solids 53(2320):2346
2. Hsu Y-F, Wang WH, Wayman CM (1999) Microstructure and martensitic transformations in a dual-phase α/β Cu-Zn alloy. Metall Mater Trans 30(729):739
3. Lee E-S, Shin TH (2011) An evaluation of the machinability of nitinol shape memory alloy by electrochemical polishing. J Mech Sci Technol 25(4):963–969
4. Telmo, Santos G, Braz Fernandes F, Bernardo G, Miranda RM (2013) Analyzing mechanical properties and nondestructive characteristics of brazed joints of NiTi shape memory alloys to carbon steel rods. Int J Adv Manuf Technol 66:787–793
5. Lei X, Rui W, Yong L (2011) The optimization of annealing and cold-drawing in the manufacture of the Ni-Ti shape memory alloy ultra-thin wire. Int J Adv Manuf Technol 55:905–910
6. Tak W, Lee M, Kim B (2011) Ultimate load and release time controllable non-explosive separation device using a shape memory alloy actuator. J Mech Sci Technol 25(5):1141–1147
7. Nam TH, Hur SG, Ahn IS (1998) Phase transformation behaviours of Ti-Ni-Cu shape memory alloy powders fabricated by mechanical alloying. Met Mater Int 4(1):61–66
8. Brook G-B (1983) Applications of titanium–nickel shape memory alloys. Mater Des 4(835):840
9. Pan W, Qin Y, Law F, Ma Y, Brockett A, Juster N (2008) Feasibility study and tool design of using shape memory alloy as tool-structural elements for forming-error compensation in microforming. Int J Adv Manuf Technol 38(3-4):393–401
10. Jee K-K, Hana J-H, Jang WY (2006) A method of pipe joining using shape memory alloys. Mater Sci Eng A 438–440(1110):1112
11. Santos TG, Fernandes FB, Bernardo G, Miranda RM (2013) Analyzing mechanical properties and non-destructive characteristics of brazed joints of NiTi shape memory alloys to carbon steel rods. Int J Adv Manuf Technol 66(787):793
12. Petrini L, Migliavacca F, Massarotti P, Schievano S, Dubini G, Auricchio F (2005) Computational studies of shape memory alloy behavior in biomedical applications. J Biomech Eng 127(716):725
13. Hartl D-J, Lagoudas D-C (2007) Aerospace applications of shape memory alloys. Proc IMechE G J Aerosp Eng 221(535):552
14. DesRoches R, Smith B (2004) Shape memory alloys in seismic resistant design and retrofit: a critical review of their potential and limitations. J Earthq Eng 8(415):429
15. Lee JK, Kim GD (2005) A theoretical comparison of two possible shape memory processes in shape memory alloy reinforced metal matrix composite. J Mech Sci Technol 19(7):1460–1468
16. Leclerq S, Lexcellent C (1996) A general macroscopic description of the thermomechanical behavior of shape memory alloys. J Mech Phys Solids 44(953):980
17. Wei ZG (1998) Transformation relaxation and aging in a CuZnAl shape-memory alloy studied by modulated differential scanning calorimetry. Metall Mater Trans A 29(11):2697–2705
18. Chu C-L, Chung C-Y, Lin P-H (2005) Characterization of transformation behaviour in porous Ni-rich NiTi shape memory alloy fabricated by combustion synthesis. J Mater Sci 40(3):773–776
19. Sepulveda A, Muñoz R, Lovey F-C, Auguet C, Isalgue A, Torra V (2007) Metastable effects on martensitic transformation in SMA (II): the grain growth effects in Cu-Al-Be alloy. J Therm Anal Calorim 89(101):107
20. Pieczyska E-A, Gadaj S-P, Nowacki W-K, Tobushi H (2006) Martensite and reverse transformation during simple shear of niti shape memory alloy. Exp Mech 46(531):542
21. Fischer F-D, Berveiller M, Tanaka K, Oberaigner E-R (1994) Continuum mechanical aspects of phase transformations in solids. Arch Appl Mech 64(54):85
22. Green A-E, Nagdhi P-M (1977) On the thermodynamics and the nature of the second law. Proc Roy Soc London A357(253):270
23. Ivshin Y, Pence T-J (1994) A thermomechanical model for a one variant shape memory material. J Intell Mater Syst Struct 5(455):473
24. Lacarbonara W, Bernardini D, Vestroni F (2004) Nonlinear thermomechanical oscillations of shape-memory devices. Int J Solids Struct 41(1209):1234
25. Mariano P-M (2002) Multifield theories in mechanics of solids. Adv Appl Mech 38(1):93
26. Otsuka K, Shimizu K (1986) Pseudoelasticity and shape memory effects in alloys. Int Metals Rev 31(93):114
27. Menezes L-F, Teodosiu C (2000) Three-dimensional numerical simulation of the deepdrawing process using solid finite elements. J Mater Process Technol 97(100):106
28. Menezes L-F (1994) Modélisation tridimensionnelle et simulation numérique des processus de mise en forme: application a' l'emboutissage des tôles métalliques. Ph.D. thesis, University of Coimbra–University of Paris 13
29. Paiva A, Savi M-A, Bragra AMB, Pacheco PMCL (2005) A constitutive model for shape memory alloys considering tensile-compressive asymmetry and plasticity. Int J Solids Struct 42(3439):3457
30. Yan W, Wang C, Zhang X, Mai Y (2003) Theoretical modelling of the effect of plasticity on reverse transformation in superelastic shape memory alloys. Mater Sci Eng A A354(146):157
31. Zhang Y, Cheng Y, Grummon D (2007) Finite element modeling of indentation-induced superelastic effect using a three-dimensional constitutive model for shape memory materials with plasticity. J Appl Phys 101(1):6
32. Wang X, Xu B-X, Yue Z (2008) Micromechanical modelling of the effect of plastic deformation on the mechanical behaviour in pseudoelastic shape memory alloys. Int J Plast 24(8):1307–1332
33. Hartl D, Lagoudas D (2009) Smart Mater Struct 18:1–17
34. Qidwai M-A, Lagoudas D-C (2000) On thermomechanics and transformation surfaces of polycrystalline NiTi shape memory alloy material. Int J Plast 16(1309):1343
35. Popov P, Lagoudas D-C (2007) A 3-D constitutive model for shape memory alloys incorporating pseudoelasticity and detwinning of self-accommodated martensite. Int J Plast 23(1679):1720
36. Arghavani J, Auricchio F, Naghdabadi R, Reali R, Sohrabpour S (2010) A 3-D phenomenological constitutive model for shape memory alloys under multiaxial loadings. Int J Plast 26(976):991
37. Mirzaeifar R, Shakeri M, Sadighi M (2009) Nonlinear finite element formulation for analyzing shape memory alloy cylindrical panels. Smart Mater Struct 12(5) doi:10.1088/0964-1726/18/3/035002
38. Mirzaeifar R, DesRoches R, Yavari A (2010) Exact solutions for pure torsion of shape memory alloy circular bars. Mech Mater 42(797):806
39. Auricchio F, Marfia S, Sacco E (2003) Modelling of SMA materials: training and two way memory effects. Comput Struct 81(2301):2317

40. Yue Z-F, Wan J-S, Zhang Q-M (2003) Rare Metal Mater Eng 32:246
41. Yan W, Wang C-H, Zhang X-P, Mai Y-W (2002) Effect of transformation volume contraction on the toughness of superelastic shape memory alloys. Smart Mater Struct 11(947):955
42. Wang X-M, Wang YF, Baruj A, Eggeler A, Yue ZF (2005) On the formation of martensite in front of cracks in pseudoelastic shape memory alloys. Mater Sci Eng A 394(393):398
43. Auricchio F, Sacco E (1997) A one-dimensional model for superelastic shape memory alloys with different elastic properties between austenite and martensite Int. J NonLinear Mech 32(1101):1114
44. Auricchio F, Sacco E (2001) Thermo-mechanical modelling of a superelastic shape-memory wire under cyclic stretching bending loadings. Int J Solids Struct 38(6123):6145
45. Gao X, Huang M, Brinson L-C (2000) A multivariant micromechanicalmodel for SMAs: part 1: crystallographic issues for single crystal model. Int J Plast 16(1345):1369
46. Thamburaja P, Anand L (2002) Superelastic behavior in tension-torsion of an initially-textured Ti-Ni shape-memory alloy. Int J Plast 18(1607):1617
47. Lim T-J, McDowell D-L (2002) Cyclic thermomechanical behavior of a polycrystalline pseudoelastic shape memory alloy. J Mech Phys Solids 50(651):676
48. Auricchio F, Taylor RL (1997) Shape-memory alloys: modelling and numerical simulations of the finite-strain superelastic behaviour. Comput Methods Appl Mech Eng 143:175–194
49. Auricchio F, Taylor R-L (1996) Shape memory alloy superelastic behavior: 3D finite element simulations. In: Proceedings of the 3rd international conference on intelligent materials, Lyon June 3-5
50. Brinson L-C (1993) One-dimensional constitutive behavior of shape memory alloys: termomechanical derivation with non-constant material functions and redefined martensite internal variable. J Intell Mater Syst Struct 4:229–242
51. Brinson L-C, Lammering R (1993) Finite element analysis of the behavior of shape memory alloys and their applications. Int J Solids Struct 30(23):3261–3280
52. Kouzak Z, Levy Neto F, Savi M-A (1998) Finite element model for composite beams using SMA fibers. In: Proceedings of CEM NNE 98 - V Congresso de Engenharia Mecânica Norte e Nordeste, vol II, Fortaleza, Brazil, 27-30 October, 112–119
53. Tanaka K (1986) A thermomechanical sketch of shape memory effect: one-dimensional tensile behavior. Res Mech 18(251):263
54. Tanaka K, Nagaki S (1982) Thermomechanical description of materials with internal variables in the process of phase transformation. Ing Arch 51(287):299
55. Auricchio F, Petrini L (2002) Improvements and algorithmical considerations on a recent three-dimensional model describing stress-induced solid phase transformation. Int J Numer Methods Eng 55(1255):1284
56. Auricchio F, Petrini L (2004) A three dimensional model describing stress-temperature induced solid phase transformations: solution algorithm and boundary value problems. Int J Numer Methods Eng 61(807):836
57. Qidwai MA, Lagoudas DC (2000) Numerical implementation of a shape-memory alloy thermomechanical constitutive model using return mapping algorithms. Int J Numer Methods Eng 47(1123):1168